ISRU Manufactured Propellants for Hall Thrusters

Lucas A., Joud B., & Tanuksh S.[1]

[1]University of Michigan, Department of Aerospace Engineering

December 12, 2025

Abstract

This research investigates using asteroid-sourced materials as propellants in a Hall effect thruster, evaluating their feasibility across key performance metrics, including achievable specific impulse, ionization energy, corrosion resistance, and suitability for deployment in deep space systems. We also examine the practicality of developing a CubeSat-scale system to harvest and store these materials for propellant use. Using a simplified Hall thruster performance model, we obtained specific impulse, propellant mass, burn time, and resource-based scores for a range of asteroid-derived materials. Results show that carbon macromolecules achieve the highest overall performance due to their availability, low corrosivity, and favorable system mass. Bismuth and iodine also rank highly, offering strong propulsion characteristics and reasonable harvesting feasibility. In contrast, noble gases score poorly due to low abundance in asteroid environments. Overall, the study indicates that carbon-rich materials and high-density metals are the most promising propellants for in-situ–resourced deep-space missions.

1 Introduction

The use of ISRU propellants is crucial to the future of space travel as mission lifetimes and distances become much longer. Evaluating key choices of propellant in the solar system will be an important first step for increasing the longevity of these missions based on availability within densely populated regions, such as asteroid belts, and their merits when utilized by Hall Effect Thrusters (HETs). Using available data from missions like *Hayabusa2* that analyzed the surface of C-type 9 (carbonaceous) asteroids in the Main Belt, we have identified several potential candidates for HET propellants, which will be evaluated based on availability and performance.

1.1 Literature Review

Studies Showing Use of Alternative Propellants for Hall Thrusters

The increasing cost and limited availability of xenon have motivated extensive research into alternative Hall thruster propellants. Two key works—Szabo et al. [1] and Tirila et al. [2]—provide valuable experimental and comparative data which together form a comprehensive picture of the current state of alternative propellant development. Their results are synthesized here along with tabulated and graphical comparisons.

1.1.1 Light Metal Propellants: Magnesium and Zinc

One of the earliest experimental demonstrations of condensable light-metal propellants for Hall thrusters was reported by Szabo et al. [1]. The authors investigated magnesium (Mg) and zinc (Zn) vapors, highlighting their

operational feasibility and their potential to achieve high specific impulse due to low atomic mass and favorable ionization properties. Vapor-fed operation was demonstrated through a wire-based propellant feed system capable of supplying Mg and Zn at controlled mass flow rates, and experiments showed stable discharges with promising thrust-to-power ratios.

Table 1 summarizes the physical and ionization properties of the major candidate propellants explored in this work and the wider literature. The strong storage-density advantages of Zn, Bi, and Cs are evident, while Mg stands out for its combination of low atomic mass and reasonable vapor pressure at moderate temperatures.

Table 1: Physical and ionization properties of selected Hall thruster propellants (from Szabo et al. [1]).

Element	**Atomic Mass**	**1st Ion. Pot. (eV)**	**Peak** σ (10^{-16}cm^2)
Mg	24.3	7.64	8.0
Zn	65.4	9.4	5.0
Kr	83.8	14.0	3.7
I	126.9	10.4	6.0
Xe	131.3	12.1	5.0
Cs	132.9	3.9	12.0
Bi	209.0	7.3	8.0

1.1.2 Comparative Assessment of Alternative Propellants

A broader multi-propellant comparison was presented by Tirila et al. [2], covering noble gases, molecular propellants, and a range of condensable species. Their 100 W station-keeping use case provides a direct comparison of mass, volume, cost, and performance across more than ten candidate propellants. Table 2 presents these results.

Table 2: Station-keeping scenario comparison for a 100 W Hall thruster (from Tirila et al. [2]).

Propellant	**Burn Time (h)**	**Mass (kg)**	**Vol (L)**	**Flow (mg/s)**	**Ideal** I_{sp} **(s)**	**Cost (USD)**
Xe	877.60	4.30	2.06	1.36	1236.24	9884.58
Kr	1089.32	3.41	3.76	0.87	1547.41	3188.26
I	892.02	4.22	0.86	1.32	1257.43	135.16
Mg	1991.89	1.81	1.04	0.25	2873.26	15.53
Zn	1228.46	3.00	0.42	0.68	1751.86	9.59
Bi	703.27	5.48	0.56	2.17	979.87	44.14
Cd	945.49	3.97	0.46	1.17	1336.04	9.87
TPA	841.69	4.50	5.98	1.48	1183.44	296.96
TEA	994.57	3.76	5.17	1.05	1408.17	563.25
C10H16	862.19	4.38	4.06	1.41	1213.59	236.67
C60	396.42	10.66	6.46	7.47	527.66	5258.24

1.2 Modeling Framework and Rationale

1.2.1 Mission Objectives and Propulsion Requirements

Deep-space missions, particularly those involving the exploration of outer Solar System bodies such as Jupiter's moons, place demanding requirements on spacecraft propulsion systems. Such missions typically require large total mission Δv, long-duration operation, and high propellant efficiency to minimize the mass launched from Earth. Solar-electric propulsion (SEP) has become increasingly favored for these trajectories, as it enables continuous low-thrust operation and significantly higher specific impulse compared to chemical propulsion.

For missions that involve refueling at intermediate targets—for instance, small asteroids located within resonant orbits or along the transfer path—the propulsion system must also operate reliably in deep-space environments, exhibit long operational lifetimes, and maintain efficiency across a wide range of power conditions. The coupling between available onboard power, propellant selection, and achievable thrust-to-power ratio therefore becomes central in identifying an appropriate propulsion architecture for such missions.

1.2.2 Hall Thrusters for Deep-Space Applications

HETs have been extensively demonstrated in Earth-surface facilities and on Earth-orbiting satellites [3] [4], and more recently on interplanetary spacecraft such as NASA's *DART* and ESA's *BepiColombo*. Hall thrusters are particularly attractive for deep-space travel due to their balance of specific impulse (typically 1200–2000s), moderate thrust levels, and relatively simple power-processing requirements compared to ion engines. Their ability to operate at sub-kilowatt to multi-kilowatt power levels also makes them well-suited for spacecraft with solar arrays that experience reduced power availability with increasing heliocentric distance.

Performance data across the literature indicate that Hall thruster characteristics scale strongly with the discharge channel geometry, including channel diameter, width, and magnetic field topology. Dimensions such as the channel area, $A = \pi h d$, have been shown to correlate with maximum stable discharge current, ionization efficiency, and overall thrust levels. Thus, selecting a set of realistic geometric parameters is essential for building an accurate analytical or computational model of thruster performance.

1.2.3 Adopting Representative Thruster Parameters

The geometric parameters used in this model are drawn from the low-assumption Hall thruster sizing study of Dannenmayer and Mazouffre [5]. Their work develops a generalized scaling method based on a broad database of existing Hall thrusters rather than a single design. This database-driven approach captures well-demonstrated trends in high-Isp, high-thrust devices across a wide range of power levels, geometries, and operating conditions. Because their analysis relies on openly available, experimentally validated thruster data, the resulting geometric relations provide a reliable and representative basis for comparative propulsion studies.

For our purposes, we adopt the *low-assumption* set of parameters reported for the 20 kW xenon case, as these are based on minimal empirical fitting and reflect more conservative and physically transparent assumptions. In particular, we borrow the input electrical power and discharge voltage $(P_{\mathrm{in}},\, V_d)$ and the resulting mean channel diameter and channel length $(d,\, L)$ given in their Table 2:

$$P_{\mathrm{in}} \approx 15\,\mathrm{kW}, \qquad V_d = 500\,\mathrm{V}, \qquad d = 324\,\mathrm{mm}, \qquad L = 51\,\mathrm{mm}.$$

The only geometric parameter not explicitly listed is the channel width h. Following the authors' mass–balance relation (their Eqs. (13)–(15)), the neutral mass flow is written as

$$\dot{m}_n \;=\; n_n\, m_n\, v_n\, A, \qquad A = \pi h d,$$

from which the channel width is obtained as

$$h \;=\; \frac{\dot{m}_n}{\pi\, n_n\, m_n\, v_n\, d}.$$

Using the low-assumption values for the mass flow rate, neutral density, thermal velocity, and xenon atomic mass reported in the study yields $h \approx 58\ \mathrm{mm}$.

By adopting these openly documented and experimentally anchored geometric scalings, our model remains general, physically interpretable, and consistent with demonstrated high-performance Hall thrusters. This provides a credible and transparent baseline for comparing the performance of different propellants under a common thruster architecture.

2 Approach

2.1 Propellant Comparison and Hall Thruster Performance Modeling

In order to compare different propellants and evaluate their performance in a given Hall thruster design, we follow a step-by-step modeling approach. The inputs to the model include the thruster operating conditions and geometric parameters:

- Input power, P_{in}
- Discharge voltage, V_d
- Channel diameter, d
- Channel length, L
- Channel width, h
- Propellant atomic mass, m_i

2.1.1 Asteroid-Derived Propellant Sources

To determine which propellants are realistically available for in-situ resource utilization (ISRU), we first examined the known spectral composition of Main Belt asteroids. C-type (carbonaceous) asteroids dominate the region, comprising approximately 75% of all bodies. Their reflectance spectra show strong hydration features and a carbon-rich surface composition. For example, the *Hayabusa2* mission's analysis of the C-type asteroid Ryugu revealed the widespread presence of OH-bearing phyllosilicates and complex organic macromolecules on the surface [6]. These organics include functional groups such as ketones, carboxyls, and aromatic rings [7], indicating carbon and oxygen as the two most abundant elements accessible for propellant production.

Mining methods depend on the material state: carbonaceous regolith can be thermally decomposed, hydrated minerals may be heated to release water, and metallic elements (e.g., iodine-, bismuth-, or tin-bearing minerals) require higher-temperature extraction or chemical separation. Once liberated, these materials can be processed into gaseous or aerosol form for Hall thruster injection.

Table 3 summarizes representative asteroid-derived propellant candidates and their key physical properties relevant to Hall thruster operation.

2.1.2 Modeling Scheme

Some preliminary calculations

Given the previous thruster geometry and operating parameters, the annular channel cross-sectional area is

$$A_{\text{ch}} \approx \pi d h = \pi(0.324)(0.058) = 0.05904\ \text{m}^2 \approx 590\ \text{cm}^2.$$

The inner and outer diameters are

$$d_{\text{in}} = d - h = 0.266\ \text{m}, \qquad d_{\text{out}} = d + h = 0.382\ \text{m},$$

giving inner and outer lateral wall areas

$$A_{\text{inner}} = \pi d_{\text{in}} L \approx 0.04262\ \text{m}^2, \qquad A_{\text{outer}} = \pi d_{\text{out}} L \approx 0.06120\ \text{m}^2.$$

Thus the total wetted wall area (inner + outer) is

$$A_{\text{wall,total}} = A_{\text{inner}} + A_{\text{outer}} = 0.10382\ \text{m}^2 \approx 1038\ \text{cm}^2.$$

Table 3: Representative asteroid-derived propellant candidates and key physical properties.

Propellant	**Mass (g/mol)**	**Ionization Energy (eV)**	**Storage Density (g/cm^3)**
Carbon macromolecules	150	11.30	1.50
Water (H_2O)	18	12.60	1.00
Hydrogen (from H_2O)	2	13.60	0.07
Oxygen (from H_2O)	32	13.60	1.43
Iodine	253	10.50	4.90
Bismuth	209	7.30	9.80
Tin	119	7.30	7.30
Sodium	23	5.10	0.97
Potassium	39	4.30	0.86
Iron	55.8	7.90	7.90
Xenon	131	12.10	0.0059
Krypton	84	14.00	0.0037

Ionization Cross–Section Estimation

Accurate evaluation of the ionization cross section σ_{iz} is required for the computation of the mass–utilization efficiency of the Hall thruster. In this work, σ_{iz} is obtained using a semi–empirical formulation based on the Lotz model, which provides an analytic approximation of electron–impact ionization cross sections for atoms and atomic ions.

Lotz Semi–Empirical Formula

For a given species with ionization potential I_j (in eV), the Lotz formula expresses the ionization cross section as a function of the incident electron energy E:

$$\sigma_{\text{iz}}(E) = \sum_j A_j \, \frac{\ln(E/I_j)}{E\, I_j} \qquad (E > I_j), \tag{1}$$

where A_j are empirical coefficients corresponding to each ionizing subshell. The cross section is zero for $E \leq I_j$.

In this study a single-term approximation is adopted for each propellant species,

$$\sigma_{\text{iz}}(E) \approx A \, \frac{\ln(E/I)}{E\, I}, \tag{2}$$

where I is the first ionization energy and A is an effective Lotz coefficient chosen to reproduce a realistic peak cross section.

Electron Energy for Evaluation

The discharge is assumed to produce an approximately Maxwellian electron population, whose characteristic electron temperature is related to the discharge voltage by

$$T_e = \alpha V_d, \tag{3}$$

with $\alpha = 0.123$ following empirical correlations used in Hall thruster plasma models. For the present operating condition ($V_d = 500$ V), this yields

$$T_e = 61.5 \text{ eV}. \tag{4}$$

To obtain a practical engineering estimate of the ionization cross section, the Lotz expression is evaluated at the characteristic electron energy,

$$\sigma_{\text{iz}} = \sigma_{\text{iz}}(E = T_e), \tag{5}$$

which provides an effective ionization cross section appropriate for use in the ionization probability and efficiency expressions. This monoenergetic approximation is commonly used in first-order Hall thruster models and gives order-of-magnitude agreement with full energy-averaged evaluations. This approach provides a consistent and reproducible estimate of σ_{iz} for all propellants considered, listed in a table in the appendix, Section 7.2.

1. **Compute Discharge Current:** The total discharge current is computed from the input power and discharge voltage:

$$I_d = \frac{P_{\text{in}}}{V_d}$$

2. **Compute Mass Utilization η_m:** The mass utilization efficiency is given by

$$\eta_m = 1 - \exp\left[-\left(\frac{I_d}{q}\right)\left(\frac{\sigma_{iz}}{u_n}\right)\left(\frac{L_{ch}}{A_{ch}}\right)\gamma N_{\text{eff}}\right] \tag{6}$$

   where q is the elementary charge, σ_{iz} is the peak ionization cross section for each propellant.

   The neutral thermal speed is evaluated assuming a Maxwellian distribution at $T_n = 800$ K:

$$u_n = \sqrt{\frac{8k_B T_n}{\pi m_n}}, \tag{7}$$

   where m_n is the neutral particle mass for each propellant.

   The ionization effectiveness factor γ is assumed to scale with ion mass according to

$$\gamma = 0.05\sqrt{\frac{0.05\, m_i}{m_e}}, \tag{8}$$

   where m_i is the ion mass and m_e is the electron mass.

   To account for electron magnetic confinement and multiple effective ionization passes, an effective interaction multiplier N_{eff} is applied. This formulation assumes singly charged ions, constant peak ionization cross sections, uniform neutral density, and effective electron recirculation captured through the single confinement parameter N_{eff}.

3. **Compute Ion Current:** Using the ionization efficiency, the resulting ion current is:

$$I_i = \eta_m I_d$$

4. **Compute Mass Flow Rate:** The mass flow rate is obtained from the ion current and propellant atomic mass:

$$\dot{m} = \frac{I_i m_i}{q}$$

5. **Compute Individual Efficiency Terms:**

Fixed Efficiency Terms

Several efficiency factors in the Hall thruster performance model are only weakly dependent on propellant species and are therefore treated as fixed parameters. Conservative values were selected based on typical ranges reported in Hall thruster literature.

Voltage and Charge Utilization

The voltage utilization efficiency η_V accounts for the fraction of discharge voltage effectively contributing to ion acceleration, while the charge utilization efficiency η_q represents the fraction of the discharge current carried by ions rather than electrons. Both are treated as propellant–independent and fixed at

$$\eta_q = \eta_V = 0.90. \tag{9}$$

These parameters allow the beam voltage to be defined directly from the discharge voltage,

$$V_b = \eta_V V_d = 0.9 \times 500\ \mathrm{V} = 450\ \mathrm{V}, \tag{10}$$

which is subsequently used in the evaluation of other efficiencies such as mass–utilization and ionization efficiency.

Divergence Efficiency

The divergence efficiency η_d accounts for the reduction in axial thrust due to plume spreading. Assuming a characteristic divergence half–angle of approximately 25°, the efficiency is fixed at

$$\eta_d = 0.82. \tag{11}$$

Cathode Efficiency

Cathode losses are modeled through a cathode efficiency term η_c, which captures the fraction of discharge power not lost to heating and electron production inefficiencies at the cathode. A conservative constant value is adopted:

$$\eta_c = 0.93. \tag{12}$$

Electrical Efficiency

Electrical efficiency η_e accounts for losses in the power-processing unit (PPU) and other electrical subsystems supplying the discharge. A typical fixed value is used for all propellants:

$$\eta_e = 0.95. \tag{13}$$

These values represent conservative but realistic performance assumptions and provide a consistent baseline for comparing propellant-dependent effects such as ionization efficiency, mass utilization, and thrust production.

Beam Utilization Efficiency

The beam utilization efficiency is modeled as

$$\eta_b = \frac{1 - \dfrac{0.5\, m_e v_e^2}{q V_b} \left(\dfrac{\nu_{en}}{\omega_{ce}}\right)^2}{1 + \dfrac{\varepsilon_{iz}}{V_b} + \sqrt{\dfrac{m_i}{m_e}}\, \delta^{3/2}\, \alpha\, \dfrac{A_{wall}}{A_{ch}}}, \tag{14}$$

where q and m_e are the electron charge and mass, m_i is the ion mass, and $V_b = \eta_v V_d$ is the effective beam voltage. The numerator accounts for electron thermal energy losses scaled by the ratio of electron–neutral collision frequency to electron cyclotron frequency, which represents the degree of magnetic confinement.

The electron thermal speed is computed assuming a single characteristic electron temperature of $T_e = 61.5\ \mathrm{eV}$,

$$v_e = \sqrt{\frac{2qT_e}{m_e}}. \tag{15}$$

This value is selected to represent energetic electrons responsible for ionization and acceleration in the discharge.

The electron–neutral collision frequency is modeled as

$$\nu_{en} = n_n \sigma_{en} v_e, \tag{16}$$

where n_n is the neutral number density and σ_{en} is approximated using the peak ionization cross section for each propellant. Magnetic confinement is represented through the electron cyclotron frequency,

$$\omega_{ce} = \frac{qB}{m_e}, \tag{17}$$

where B is the applied magnetic field strength. The ratio $(\nu_{en}/\omega_{ce})^2$ therefore quantifies the competition between collisional scattering and magnetic confinement.

Fixed empirical loss factors are applied with $\delta = 0.1$ representing sheath–divergence losses and $\alpha = 0.05$ representing wall loss effects.

The ionization energy loss term ε_{iz} represents the mean energy required per ion produced. For noble gas propellants (Xe, Kr, Ar), measured mean ion-pair energies W from the literature are used. For all other species, ε_{iz} is estimated by scaling the first ionization potential I according to

$$\varepsilon_{iz} = We, \qquad W = \kappa_W I, \qquad \kappa_W = 2.5, \tag{18}$$

where I is in electron-volts and e is the elementary charge. This scaling accounts for additional excitation and inelastic energy losses beyond first ionization and enables a consistent treatment of metallic and molecular propellants.

6. **Compute Total Efficiency:** The total utilization efficiency is obtained as the product of individual efficiencies:

$$\eta_{\mathrm{total}} = \eta_m \eta_q \eta_v \eta_c \eta_d \eta_e \eta_b$$

7. **Compute Effective Exhaust Velocity:** The exhaust velocity is determined using the total efficiency and power input:

$$v_{eff} = \sqrt{\frac{2\eta_{\mathrm{total}} P_{\mathrm{in}}}{\dot{m}}}$$

8. **Compute Thrust:** Thrust can be computed either from momentum or from an empirical power relation:

$$T = \dot{m} v_e \quad \text{or} \quad T = \sqrt{2\eta_{\mathrm{total}} P_{\mathrm{in}} \dot{m}}$$

9. **Compute Specific Impulse:** The specific impulse is obtained either from thrust and mass flow rate or the effective exhaust velocity:

$$I_{\mathrm{sp}} = \frac{T}{\dot{m} g_0} \quad \text{or} \quad I_{\mathrm{sp}} = \frac{v_{\mathrm{eff}}}{g_0}$$

3 Mission Architecture Summary

A clear definition of the mission architecture is required to establish the total Δv budget, which directly informs propellant selection and Hall thruster operating regimes. Because the trajectory relies on continuous low-thrust spirals rather than impulsive chemical burns, the choice of propellant strongly affects mass fraction, transfer strategy, and overall feasibility. For this study, we assume the spacecraft begins the mission already inserted into a 200 km circular Low Earth Orbit (LEO). The goal of the mission is to depart LEO, utilize a Mars gravity assist, refuel within the inner main asteroid belt, and ultimately capture into orbit around Jupiter and transfer to Ganymede. The full architecture is summarized below and shown in Fig1.

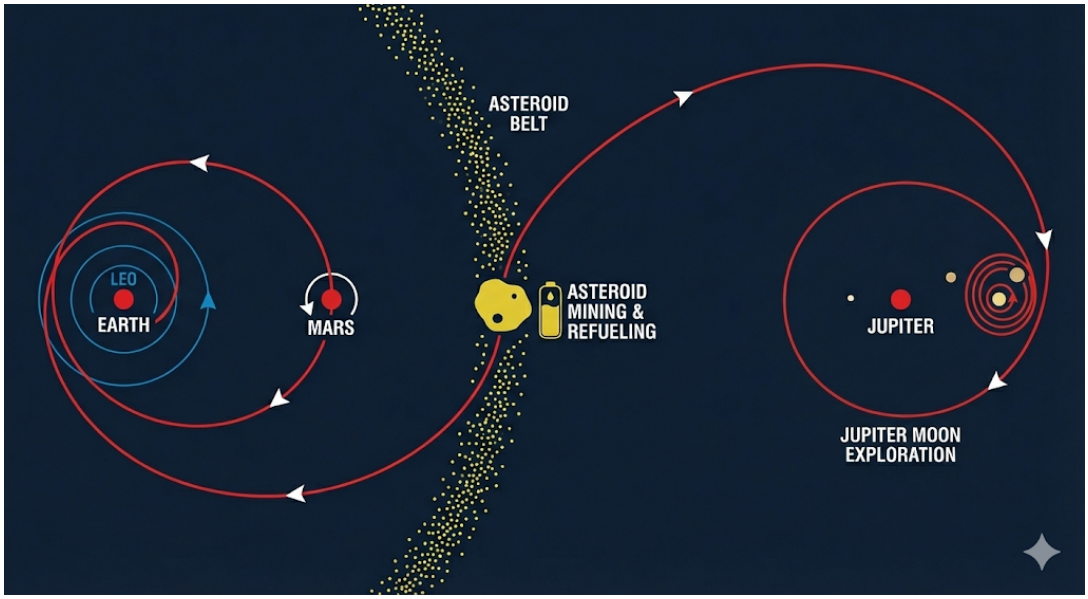

Figure 1: Image generated by Gemini (Google) showing a simplified trajectory of the mission

3.1 Mission Architecture Overview

1. LEO Departure

- **Initial Orbit:** 200 km circular LEO (assumed starting condition)
- Δv**:** ~ 4 km/s, including low-thrust spiral losses
- **Notes:** Continuous thrusting is used to spiral outward and achieve Earth escape.

2. Earth to Mars Transfer

- **Trajectory:** Low-thrust interplanetary spiral, Hohmann-like in geometry
- Δv**:** ~ 3.5 km/s
- **Notes:** Continuous thrust allows gradual acceleration and potential plane adjustments to position the spacecraft for the Mars gravity assist and later belt rendezvous.

3. Mars Gravity Assist

- **Purpose:** Increase heliocentric velocity in the direction of Jupiter and reduce the required Δv for the outbound leg by $\sim$ 1–2 km/s

4. Inner Main Belt Refueling Stop

- **Location:** 2.2–2.5 AU
- **Candidate Targets:** Hygiea, Interamnia, Eunomia, Eos/Koronis family
- Δv **to rendezvous:** 0.5–1.0 km/s (low-thrust orbit matching)
- **Refueling:** Extraction of propellant
- **Notes:** This refueling opportunity drastically reduces initial LEO mass requirements and increases payload fraction by allowing the spacecraft to depart LEO with only partial propellant load.

5. Inner Belt to Jupiter Transfer

- **Trajectory:** Outbound low-thrust spiral assisted by the earlier Mars flyby
- Δv**:** ~ 4.5 km/s
- **Notes:** Continuous thrust provides gradual outward acceleration and trajectory shaping required for Jupiter approach and capture.

6. Jupiter Capture

- **Method:** Low-thrust braking and gradual orbit insertion
- Δv**:** $\sim$ 2.5–3 km/s
- **Notes:** Electric propulsion enables a gentle capture strategy, reducing propellant demand relative to impulsive chemical capture.

7. Transfer to Ganymede

- Δv**:** ~ 0.3 km/s
- **Notes:** Includes circularization and approach trajectory shaping for scientific operations in Ganymede orbit.

8. Final Mission State

- **End Orbit:** Stable operational orbit around Ganymede
- **Total Conservative** Δv**:** 9km/s for the first portion (Earth–Asteroid), and 8km/s for the second portion (Asteroid–final orbit) (includes a 10% margin)

This architecture highlights why accurate Δv modeling is a prerequisite for propellant selection. Different propellants and operating points will affect thrust, specific impulse, and mass fraction, thereby influencing transfer durations, refueling frequency, and the overall feasibility of the deep-space trajectory.

4 Results

The code repeats the above steps for each propellant of interest shown in table 3 using their atomic mass and ionization properties.

4.1 Performance Parameters from the model

The resulting thrust, specific impulse, and efficiencies of the thruster running on the different propellants are shown in the following table:

Table 4: Performance Parameters for Various Propellants

Propellant	$\dot{m}$ (mg/s)	I_{sp} (s)	Thrust (mN)	Total Efficiency
I_2	78.92	1091.88	845.01	0.3016
Carbon Macros	46.64	1507.54	689.51	0.3398
Bi	64.98	1231.33	784.62	0.3158
Sn	36.91	1735.42	628.16	0.3564
Na	7.15	4464.87	312.99	0.4568
K	12.16	3313.89	395.07	0.4280
H_2O	5.60	5109.15	280.65	0.4687
H–water	0.62	16479.4	100.49	0.5414
O–water	9.95	3711.24	362.12	0.4393
Kr	26.06	2133.58	545.16	0.3802
Xe	40.82	1633.68	654.02	0.3493
Fe	17.36	2702.39	460.16	0.4065

4.2 Propellant Trade Study

To evaluate propellants for long-duration Hall thruster missions, we conducted a trade study incorporating corrosivity, availability within asteroid regolith, storage density, and the practical difficulty of harvesting the material in situ. C-type asteroids favor carbon- and oxygen-bearing compounds, which are abundant and easier to liberate thermally. Metallic propellants such as iodine, bismuth, and tin offer attractive physical properties (high atomic mass, high storage density, and relatively low ionization energy), but they are far less abundant in carbonaceous bodies and require high-temperature extraction followed by conversion to a vapor or aerosol suitable for Hall thruster injection. These solid-state handling challenges reduce their overall score despite favorable performance metrics.

Carbon macromolecules (benzenes, organics, polycyclic aromatic hydrocarbons, etc. [6]) remain the most abundant propellant source, though their high ionization energy and molecular complexity make them less ideal for efficient plasma generation. Water and its derivative products (H_2 and O_2) are moderately abundant and exceptionally easy to harvest, especially from hydrated minerals identified on Ryugu and other C-type objects. Noble gases such as Xe and Kr have extremely low availability and difficult harvesting requirements, resulting in low total scores despite their ideal ionization properties.

The weighted scoring approach used here incorporates the same parameter weights shown in Table 5. Lower ionization energy corresponds to a higher score using an inverted $(1/IE)$ weighting.

In Table 5 Density, Availability and Harvest Ease are weighted positively following $Value * Weight$, while M_p, Burn Time, and Corrosivity are weighted inversely such that higher values result in a lower score following $(1/Value) * Weight$. Values for M_p and Burn Time are normalized following Equation 19 to contribute a value ranging from 0-6 to the overall material score.

$$w\left(\frac{x - x_{\min}}{x_{\max} - x_{\min}} \times 6\right) \tag{19}$$

4.2.1 Propellant Mass and Burn Time Estimation

To size the propulsion system for the Jovian moon mission, we begin by estimating the total propellant mass required to deliver the spacecraft's characteristic velocity increment. From preliminary trajectory analysis, each phase of the mission requires a total $\Delta v \approx 9\ \mathrm{km/s}$, delivered by a 15 kW Hall thruster.

Propellant Mass Estimation

For electric propulsion, the rocket equation remains valid, but because the thrust is very low, we treat Δv as accumulated quasi-continuously over a long spiral trajectory. The Tsiolkovsky relation is

$$\Delta v = I_{\mathrm{sp}} g_0 \ln\left(\frac{m_0}{m_f}\right), \tag{20}$$

where I_{sp} is the specific impulse of the chosen propellant, m_0 is the initial mass, and m_f is the final (dry) mass. Rearranging for the required propellant mass M_p,

$$M_p = m_0 - m_f = m_f\left(\exp\left(\frac{\Delta v}{I_{\mathrm{sp}} g_0}\right) - 1\right). \tag{21}$$

We assume a realistic dry mass representative of a small interplanetary electric-propulsion spacecraft. For this study we adopt

$$m_f = 800\ \mathrm{kg}, \tag{22}$$

which includes the spacecraft bus, solar arrays, mining equipment, structure, and margins.

Burn Time Estimation

Propellant	**Density** ($\frac{g}{cm^3}$)	M_p **(kg)**	**BurnTime (days)**	**Availability**	**Corrosivity**	**Harvest Ease**	**Total Score**
Parameter Weights	0.3	0.4	0.1	0.9	0.8	0.6	–
Carbon–macromolecules	1.5	670.23	166.32	5	1	3	**7.245364**
Water (H_2O)	1.0	157.36	325.23	4	4	6	**4.484324**
H (from H_2O)	0.07	45.8	1018	3	1	3	**4.121000**
O (from H_2O)	1.43	224.36	191	3	3	3	**3.846290**
Iodine	4.9	1053.52	154.5	2	3	3	**6.070000**
Bismuth	9.8	885.28	157.68	2	2	1	**7.141527**
Tin	7.3	557.31	174.76	1	1	1	**5.122297**
Sodium	0.97	182.49	295.4	3	5	3	**3.681113**
Potassium	0.86	255.17	242.87	3	5	3	**3.678042**
Iron	7.9	323.38	215.6	3	5	1	**5.933544**
Xenon	0.0059	602.74	170.9	0.5	0.5	0.5	**3.389582**
Krypton	0.0037	429.8	190.89	0.5	0.5	0.5	**2.990935**

Table 5: Propellant trade table using updated parameters, weights, and totals from recalculated spreadsheet. Propellant Mass and Burn Time columns normalized to value 0-6 for score calculation. Corrosivity, Propellant Mass and Burn time weighted inversely.

The Hall thruster produces a (roughly) constant thrust during the spiral-out phases. For a thruster generating T Newtons and consuming propellant at a mass flow rate $\dot{m}$, the total burn time is

$$t_{\text{burn}} = \frac{M_p}{\dot{m}}. \tag{23}$$

Where the propellant mass is obtained directly from the Tsiolkovsky equation and an assumed dry mass, while the burn time follows from the mass of propellant required and mass flow rate relations for electric propulsion. These relations form the foundation for sizing the spacecraft and evaluating the feasibility of multi-leg refueling operations during the transit to the Jovian system.

5 Discussion

The results of this study highlight both the promise and the limitations of using asteroid-derived materials as Hall thruster propellants. While the unified performance model provides a consistent basis for comparing highly diverse species, several simplifying assumptions introduce uncertainties that influence the ranking of propellant candidates.

Implications of the Results

The emergence of carbon macromolecules, bismuth, and iodine as the most favorable propellants suggests that future in-situ resource utilization (ISRU) architectures would benefit from targeting carbonaceous (C-type) and metal-rich asteroids with extractable volatiles or refractory inclusions. The high viability of carbonaceous material is especially noteworthy because it ties propulsion performance directly to the most common asteroid class in the Main Belt, strengthening the case for scalable ISRU propulsion systems. Bismuth's strong performance confirms trends observed in laboratory Hall thrusters, where high-density metals provide high thrust and moderate Isp at fixed power. The model also reinforces the long-standing attractiveness of iodine as a xenon alternative due to its high storage density, solid-state containment, and efficient propellant utilization.

Unexpected Trends and Their Interpretation

One unexpected outcome is the comparatively strong ranking of carbon macromolecules. Carbon is not conventionally considered a Hall thruster propellant, and its good performance here arises from a combination of low ionization energy, high availability, and favorable storage properties. This highlights how access-driven metrics can outweigh purely plasma-performance metrics when evaluating ISRU propellants.

Another noteworthy trend is the weaker-than-expected performance of water-derived hydrogen and oxygen. While water is among the most commonly cited ISRU materials, the need for electrolysis and cryogenic or pressurized storage significantly reduces its overall system-level attractiveness. This shows that abundance alone is insufficient: the processing chain must also be power-efficient and compatible with spacecraft thermal constraints.

Sources of Error and Modeling Limitations

Several simplifying assumptions introduce uncertainty into the absolute values of specific impulse, mass flow rate, and burn duration:

- **Ionization Cross Sections:** The use of a monoenergetic Lotz-based estimate evaluated at a single electron temperature (61.5 eV) neglects the full Maxwellian distribution. True energy-averaged cross sections would vary, especially for metals with complex electronic structure.
- **Neutral Density and Flow Uniformity:** A spatially uniform neutral density is assumed, whereas real Hall thrusters exhibit strong gradients due to depletion, recirculation, and wall interactions. This affects mass utilization and the computed discharge-to-ion current ratio.

- **Beam Utilization Efficiency Approximations:** The beam efficiency model uses fixed factors for plume divergence, sheath effects, and excitation losses. The largest uncertainty here is the scaling of mean ionization energy for non-noble gases, which may under- or over-estimate energy losses for molecular or metal species.
- **No Multi-Charge States:** Only singly ionized ions are included. Some metals (e.g., Bi, Fe) can produce multiply-charged ions that increase specific impulse but also increase erosion and power cost.
- **ISRU Extraction Energetics Not Fully Modeled:** Extraction temperatures, mining power, purification steps, and on-board storage thermal loads are estimated qualitatively rather than modeled quantitatively, introducing uncertainty into the "Harvest Ease" score.

These assumptions introduce systematic error into the final performance metrics. However, because all propellants are evaluated under the same framework, the *relative* ranking remains meaningful even if absolute values carry uncertainty.

Future Improvements

This modeling framework can be improved through several refinements:

- Implementing full energy-averaged ionization cross sections using Maxwellian distributions.
- Incorporating spatially resolved neutral and electron density profiles from a simplified fluid or hybrid PIC model.
- Including material sputtering, erosion rates, and channel wear models to better capture corrosivity effects.
- Coupling the propulsion model to a quantitative ISRU power model to compute the true system-level cost of processing each propellant.
- Simulating multi-charge effects and excitation/ionization cascades for metals and molecular species.

Together, these improvements would reduce uncertainty in the performance predictions and provide a more accurate basis for selecting asteroid-based propellants in future deep-space missions.

6 Conclusion

Using a unified performance and resource-accessibility model, this study evaluated a range of asteroid-derived materials as Hall thruster propellants and quantified their relative viability for deep-space electric propulsion. When all factors were combined—including specific impulse, required propellant mass, burn duration, storage density, corrosivity, and in-situ harvesting feasibility—the results showed a clear ordering of preferred propellants.

Carbon macromolecules emerged as the top-performing option, driven by their high availability on carbonaceous asteroids, reasonably high specific impulse, low corrosivity, and moderate extraction requirements. **Bismuth ranked second**, offering high density and strong thruster performance with manageable storage behavior. **Iodine followed closely**, benefitting from solid-state storage, moderate harvesting difficulty, and well-characterized Hall thruster performance.

By comparison, water-derived hydrogen and oxygen performed well in terms of availability but were limited by high power requirements and lower effective performance. Tin, iron, sodium, potassium, xenon, and krypton were found to be less favorable overall due to a combination of lower availability, higher corrosion risk, or challenging extraction conditions.

Overall, the results demonstrate that **carbon macromolecules, bismuth, and iodine** are the most promising candidates for asteroid-sourced Hall thruster propellants. These findings support the feasibility of in-situ propellant production for long-duration missions and provide a quantitative basis for selecting resource targets and propulsion system designs in future deep-space missions.

References

[1] J. Szabo, M. Robin, R. Conversano, and V. Hruby, "Light metal propellant hall thrusters," in *44th AIAA/ASME/SAE/ASEE Joint Propulsion Conference & Exhibit*, 2009. IEPC-2009-138.

[2] J. Tirila, S. Vannoo, S. Scharfe, P. Liang, P. Grondein, Z. S. Olsen, S. Mazouffre, and D. Lundin, "Review of alternative propellants in hall thrusters," *Acta Astronautica*, vol. 213, pp. 324–353, 2023.

[3] W. Huang, J. H. Gilland, D. A. Herman, L. Zuo, C. Feng, P. Wright, I. Johnson, C. Mullins, and K. Hohman, "A facility effect characterization test of the bht-6000 hall thruster," *AIAA SciTech Forum Conference Proceedings*, 2024. NASA Glenn Research Center Report / NTRS 20230015321.

[4] SETS, "St-100 hall-effect thruster for large satellites." `https://sets.space/st-100-hall-effect-thruster-for-large-satellites/`, 2024. Accessed: YYYY-MM-DD.

[5] K. Dannenmayer and S. Mazouffre, "Elementary scaling laws for sizing up and down hall effect thrusters: Impact of simplifying assumptions," in *Proceedings of the 31st International Electric Propulsion Conference (IEPC)*, (Ann Arbor, Michigan, USA), 2009. IEPC Paper 2009-077.

[6] e. a. K. Kitazato, "The surface composition of asteroid 162173 ryugu from hayabusa2 near-infrared spectroscopy," *Science*, 2019.

[7] e. a. Shui XU, "Small main-belt asteroid spectroscopic survey: Initial results," *ScienceDirect*, 1995.

7 Appendix

7.1 A:Model Code

```
"""
    /.
Authored by: Joud Bamehriz
Refernces used are in the refernces section of the report
"""
import math
from collections import OrderedDict

# -------------------------
# Physical Constants
# -------------------------
q_e = 1.602176634e-19       # elementary charge (C)
k_B = 1.380649e-23          # Boltzmann constant (J/K)
amu_kg = 1.66053906660e-27  # atomic mass unit (kg)
m_e = 9.1093837015e-31      # electron mass (kg)
pi = math.pi
g_0= 9.80665                #acceleration of gravity (m/s^2)

# -------------------------
# Thruster Inputs
# -------------------------
Pin = 15e3       # input power (W), changing this changes thrust but not Isp
```

```
Vd = 500.0       # discharge voltage (V)
L_ch = 0.051     # channel length (m)
d = 0.324        # diameter (m)
h = 0.058        # channel height (m)
A_ch = math.pi * d * h
T_neutral = 800.0  # neutral temperature (K)

# ------------------------
# Propellant Table
# ------------------------
species = OrderedDict([
    ("I2",  {"mass_amu": 2*126.90447, "sigma": 8.00e-20}),
    ("Carbon macro", {"mass_amu":150, "sigma":7.00e-20}),
    ("Bi",  {"mass_amu": 208.98040,    "sigma": 8.50e-20}),
    ("Sn",  {"mass_amu": 118.710,      "sigma": 5.00e-20}),
    ("Na",  {"mass_amu": 22.98976928,  "sigma": 1.50e-20}),
    ("K",   {"mass_amu": 39.0983,      "sigma": 2.00e-20}),
    ("H2O", {"mass_amu": 18.01528,     "sigma": 1.50e-20}),
    ("H_water", {"mass_amu": 2, "sigma":1.05e-20}),
    ("O_water", {"mass_amu": 32, "sigma":1.36e-20}),
    ("Ar",  {"mass_amu": 39.948,       "sigma": 2.50e-20}),
    ("Kr",  {"mass_amu": 83.798,       "sigma": 4.00e-20}),
    ("Xe",  {"mass_amu": 131.293,      "sigma": 6.00e-20}),
    ("Fe",  {"mass_amu": 55.845,       "sigma": 4.00e-20}),
])

# ------------------------
# Step 1: Discharge Current
# ------------------------
Id = Pin / Vd   # [A]

# ------------------------
# Helper Functions
# ------------------------
def neutral_thermal_speed(mass_amu, T):
    m_n = mass_amu * amu_kg
    return math.sqrt((8.0 * k_B * T) / (pi * m_n))

def gamma_model(mass_amu):
    m_i = mass_amu * amu_kg
    return 0.05 * math.sqrt((m_i * 0.05) / m_e)
N_eff = 1000   # effective electron pass multiplier
def mass_utilization_eta(Id, sigma_iz, u_n, Lch, Ach, gamma):
    exponent = - (Id / q_e) * (sigma_iz / u_n) * (Lch / Ach) * gamma* N_eff
    return 1.0 - math.exp(exponent)
m_i_d= {}
for name, props in species.items():
    mass_amu = props["mass_amu"]

    m_i_d[name] = mass_amu * amu_kg
```

```
    print(m_i_d[name])


# ------------------------------------
# Self-consistent solution for N_eff, eta_m, and mdot
# ------------------------------------

# Precompute per-species neutral speeds and gammas
u_n_dict = {}
gamma_vals = {}
for name, props in species.items():
    mass_amu = props["mass_amu"]
    u_n_dict[name] = neutral_thermal_speed(mass_amu, T_neutral)
    gamma_vals[name] = gamma_model(mass_amu)

# Initial guesses
N_eff_dict = {}
eta_m = {}
for name in species:
    N_eff_dict[name] = 100.0   # initial guess
    eta_m[name] = 0.5          # seed value

# Iterate to converge N_eff → m → mdot → n_n → N_eff
for iteration in range(15):

    # 1) Compute m using current N_eff_dict
    for name, props in species.items():
        sigma = props["sigma"]
        eta_m[name] = mass_utilization_eta(
            Id,
            sigma,
            u_n_dict[name],
            L_ch,
            A_ch,
            gamma_vals[name] * N_eff_dict[name]   # only change here
        )

    # 2) Compute mdot from m
    mdot = {}
    for name, props in species.items():
        m_i = props["mass_amu"] * amu_kg
        I_i_val = eta_m[name] * Id
        mdot[name] = I_i_val * m_i / q_e

    # 3) Compute new neutral density n_n
    n_n = {}
    for name, props in species.items():
        m_i = props["mass_amu"] * amu_kg
        n_n[name] = mdot[name] / (m_i * u_n_dict[name] * A_ch)
```

```
    # 4) Update N_eff based on mean free path
    for name, props in species.items():
        sigma = props["sigma"]
        if n_n[name] > 0:
            lambda_mfp = 1.0 / (n_n[name] * sigma)
        else:
            lambda_mfp = 1e12

        P_iz = L_ch / (L_ch + lambda_mfp)
        P_iz = max(P_iz, 1e-12)
        N_eff_dict[name] = 1.0 / P_iz

# Replace your scalar N_eff with per-species dictionary
N_eff = N_eff_dict

# Print results for confirmation
for name in species:
    print("_m for", [name], eta_m[name])
    print("mdot for", [name], mdot[name])
    print("N_eff for", [name], N_eff[name])

# -------------------------
# Step 5a: Fixed Efficiency Terms
# -------------------------
eta_q = {}
eta_v = {}
eta_d = {}
eta_c = {}
eta_e = {}


for name in species:
    eta_q[name] = 0.9   # Charge utilization efficiency (fixed)
    eta_v[name] = 0.9   # Voltage utilization efficiency (fixed)
    eta_d[name] = 0.82   # Divergence efficiency (fixed assuming a divergence ang
    eta_c[name] = 0.93   # Cathode efficiency (fixed)
    eta_e[name] = 0.95   # Electrical efficiency (fixed)

# -------------------------
# Step 5b: Beam Efficiency _b
# -------------------------

# Fixed beam-loss model constants
delta = 0.1       # sheath / divergence factor
alpha = 0.05      # wall loss factor
T_e = 800.0       # electron temperature [K]

# Electron thermal speed (at 800 K)
v_e = math.sqrt((8.0 * k_B * T_e) / (pi * m_e))
```

```
# Wall area estimate (cylindrical channel walls)
A_wall = math.pi * d * L_ch

# -------------------------
# Ionization Energy Model _iz
# -------------------------

# First ionization energies from your table (eV)
I_eV = {
    "I2": 10.45,
    "Carbon macro": 11.30,
    "Bi": 7.29,
    "Sn": 7.34,
    "Na": 5.14,
    "K": 4.34,
    "H2O": 12.60,
    "H_water": 13.60,
    "O_water": 13.60,
    "Ar": 15.76,
    "Kr": 14.00,
    "Xe": 12.13,
    "Fe": 7.90
}

# Literature mean energy per ion pair W (eV) for noble gases
W_literature = {
    "Xe": 21.9,
    "Kr": 23.6,
    "Ar": 26.3
}

# Fallback scaling factor for non-noble species
kappa_W = 2.5

# Energy cost per ion (J)
epsilon_iz = {}

for name in species:
    if name in W_literature:
        W_eV = W_literature[name]
    else:
        W_eV = kappa_W * I_eV[name]

    epsilon_iz[name] = W_eV * q_e  # [J]


# -------------------------
# Beam Efficiency _b
# -------------------------
```

```
# Fixed electron temperature
T_e_eV = 61.5
T_e_J = T_e_eV * q_e

# Electron thermal speed from kinetic energy
v_e = math.sqrt(2.0 * T_e_J / m_e)

# Magnetic field & neutral density
B_field = 0.02    # [T]

# Dictionary to store neutral densities
n_n_d = {}

for name, props in species.items():
    # Mass of ion for this species
    m_i_local = m_i_d[name]

    # Recompute neutral thermal speed for each species
    u_n_local = neutral_thermal_speed(props["mass_amu"], T_neutral)

    # Compute neutral number density
    n_n_d[name] = mdot[name] / (m_i_local * u_n_local * A_ch)



# Wall area
A_wall = math.pi * d * L_ch

eta_b = {}

for name, props in species.items():

    m_i = props["mass_amu"] * amu_kg
    V_b = eta_v[name] * Vd
    eps_iz = epsilon_iz[name]

    # -------------------------
    # Electron-neutral collision frequency
    # _en = n_n * _en * v_e
    # -------------------------
    sigma_en = props["sigma"]        # using ionization cross-section as estimate
    n_n = n_n_d[name]
    nu_en = n_n * sigma_en * v_e    # [1/s]

    # -------------------------
    # Electron cyclotron frequency
    # _ce = qB / m_e
    # -------------------------
    omega_ce = q_e * B_field / m_e  # [rad/s]
```

```
    # -------------------------
    # Magnetization scaling (/)^2
    # -------------------------
    if omega_ce > 0:
        mag_scale = (nu_en / omega_ce)**2
    else:
        mag_scale = 0.0

    # -------------------------
    # Corrected, dimensionless numerator
    # -------------------------
    if V_b > 0:
        num = 1.0 - (0.5 * m_e * v_e**2 / (q_e * V_b)) * mag_scale
    else:
        num = 0.0

    # -------------------------
    # Denominator
    # -------------------------
    term_ionization = eps_iz / V_b if V_b > 0 else float('inf')
    term_wall = math.sqrt(m_i / m_e) * (delta**1.5) * alpha * (A_wall / A_ch)
    den = 1.0 + term_ionization + term_wall

    # -------------------------
    # Safe beam efficiency
    # -------------------------
    eta_raw = num / den if den != 0 else 0.0
    eta_b[name] = max(0.0, min(1.0, eta_raw))

# -------------------------
# Total Efficiency _total
# -------------------------
eta_total = {}

for name in species:
    eta_total[name] = eta_q[name] * eta_v[name] * eta_d[name]*eta_e[name] * eta_
    print('The total efficiency for', [name], 'is', eta_total[name])


# -------------------------
# At this step we have a total efficiency that can be used to compute Thrust, Isp
# -------------------------

# -------------------------
# Exhaust velocity for each propellant
# -------------------------
v_ex= {}

for name in species:
    v_ex[name] = math.sqrt((2*eta_total[name]*Pin)/(mdot[name]))
```

```
    print('Effective exaust velocity for', [name], v_ex[name])

# -------------------------
# Momentum based thrust
# -------------------------
T_m= {}

for name in species:
    T_m[name] = mdot[name]*v_ex[name]
    print('momentum based thrust for', [name], 'is', T_m[name],'Newtons')

# -------------------------
# Power based thrust (same as momentum based, but wanted to double check)
# -------------------------
T_p= {}

for name in species:
    T_p[name]=math.sqrt(2*eta_total[name]*Pin*mdot[name])

# -------------------------
# Specific Impulse
# -------------------------
I_sp= {}

for name in species:
    I_sp[name]=v_ex[name]/g_0
    print('Specific Impulse for', [name], 'is', I_sp[name], 'seconds')
```

7.2 B: Intermediate Calculations

Table 6: Lotz Model Parameters Used for Ionization Cross–Section Evaluation

Species	I **(eV)**	$E_{\text{peak}} = 2.72\,I$ **(eV)**	σ_{peak} **(m^2)**	S **(m^{2}eV)**
Iodine (I_2)	10.45	28.42	8.00×10^{-20}	2.274×10^{-18}
Bismuth (Bi)	7.29	19.83	8.50×10^{-20}	1.685×10^{-18}
Tin (Sn)	7.34	19.96	5.00×10^{-20}	9.982×10^{-19}
Sodium (Na)	5.14	13.98	1.50×10^{-20}	2.097×10^{-19}
Potassium (K)	4.34	11.80	2.00×10^{-20}	2.361×10^{-19}
Water (H_2O)	13.60	36.99	1.50×10^{-20}	5.549×10^{-19}
Argon (Ar)	15.76	42.87	2.50×10^{-20}	1.072×10^{-18}
Krypton (Kr)	14.00	38.08	4.00×10^{-20}	1.523×10^{-18}
Xenon (Xe)	12.13	32.99	6.00×10^{-20}	1.980×10^{-18}
Iron (Fe)	7.90	21.49	4.00×10^{-20}	8.595×10^{-19}

Nomenclature

α	Wall-loss scaling factor
Δv	Required velocity change (m/s)
δ	Sheath-divergence loss factor
$\dot{m}$	Mass flow rate (kg/s)
ϵ_{iz}	Ionization energy loss per ion (J)
η_b	Beam utilization efficiency
η_c	Cathode efficiency
η_d	Divergence efficiency
η_e	Electrical efficiency
η_m	Mass utilization efficiency
η_q	Charge utilization efficiency
η_v	Voltage utilization efficiency
η_{total}	Total thruster efficiency
γ	Ionization effectiveness factor
κ_W	Ionization-energy scaling constant
ν_{en}	Electron–neutral collision frequency (s^{-1})
ω_{ce}	Electron cyclotron frequency (rad/s)
σ_{iz}	Ionization cross section (m^2)
A_{ch}	Channel cross-sectional area (m^2)
a_{sc}	Spacecraft acceleration (m/s^2)
A_{wall}	Total wetted wall area (m^2)
B	Magnetic field strength (T)
d	Mean channel diameter (m)
g_0	Standard gravity, $9.80665\ \text{m}/\text{s}^2$
h	Channel width (m)
I_d	Discharge current (A)
I_i	Ion current (A)
I_{sp}	Specific impulse (s)

k_B	Boltzmann constant (J/K)
L_{ch}	Channel length (m)
m_e	Electron mass (kg)
m_i	Ion mass (kg)
M_p	Total propellant mass required (kg)
m_{dry}	Spacecraft dry mass (kg)
n_n	Neutral number density (m^{-3})
N_{eff}	Electron recirculation multiplier
P_{in}	Thruster input power (W)
q_e	Elementary charge (C)
T	Thrust (N)
T_e	Electron temperature (eV)
T_n	Neutral gas temperature (K)
t_{burn}	Total burn time (s or days)
u_n	Neutral thermal velocity (m/s)
V_b	Effective beam voltage, $\eta_v V_d$ (V)
V_d	Discharge voltage (V)
v_{eff}	Effective exhaust velocity (m/s)
W	Mean ion-pair energy (eV)